

Distance Spectrum of IEEE 802.11 Binary Convolutional Codes

Rethna Pulikkoonattu

rethna@broadcom.com

Binary convolutional coding (BCC) has been a cornerstone of the IEEE 802.11 wireless LAN standard since its inception, and it remains relevant today across the full generational arc from the legacy 802.11a/g through Wi-Fi 6 (802.11ax) and into the forthcoming Wi-Fi 8 (802.11bn) [10, 11]. Although low-density parity-check (LDPC) codes now dominate high-throughput applications, BCC is mandatory for backward compatibility and continues to serve as the *default* forward-error-correction scheme in bandwidth-constrained and cost-sensitive deployments: 20 MHz-only devices, Internet-of-Things nodes, and other implementations where LDPC's decoder complexity is prohibitive. Critically, BCC at rate $1/2$ is the coding scheme used throughout the packet preamble in every IEEE 802.11-compliant frame, making it indispensable regardless of which data-field code is selected. Furthermore, the new *Enhanced Long Range* (ELR) packet format introduced in the 802.11bn/UHR amendment mandates rate- $1/2$ BCC for the data portion of the frame, reinforcing the continued importance of this code in next-generation deployments [11].

The performance of BCC under Viterbi decoding is governed by the *distance spectrum* $\{(\alpha_d, \beta_d)\}_{d \geq d_{\text{free}}}$ of the convolutional code [12, 16]. This note explains how to compute that spectrum exactly for the IEEE 802.11 mother code (rate $1/2$, $K = 7$, generators $133_8/171_8$) and its three standard punctured derivatives (rates $2/3$, $3/4$, $5/6$) obtained via rate-compatible puncturing [2, 8]. Union-bound BEP and FER curves are derived for AWGN with BPSK/QPSK and Gray-coded M -QAM modulation and validated against Monte Carlo simulation. Python, Julia, and C++ implementations are openly available at [7].

Introduction

Despite the ubiquity of BCC in deployed IEEE 802.11 systems, a recurring obstacle when analysing or benchmarking its performance is the absence of a self-contained, publicly accessible resource that derives the distance spectrum from first principles and connects it cleanly to BER and FER bounds. Existing textbook treatments [12, 14, 17] cover the theory at varying levels of generality but do not provide spectrum tables, working code, or simulation-validated bound curves specific to the 802.11 puncture schedules. Standards documents [10] state the generator polynomials and puncture matrices but say nothing about performance analysis. This leaves practitioners either re-deriving the computation from scratch or relying on unverified figures scattered across the literature.

This report attempts to fill that gap. The distance spectrum for each of the four standard rates is tabulated exactly; union-bound BEP and FER curves are derived and cross-validated against Monte Carlo simulation for both QPSK and 256-QAM; and the complete computational procedure is documented in pseudocode and three reference implementations (Python, Julia, C++). We hope the docu-

The resulting trellis [6] has $2^{K-1} = 64$ states, each with exactly two outgoing branches (for $u \in \{0, 1\}$).

Figure ?? shows the first four states over seven time steps.

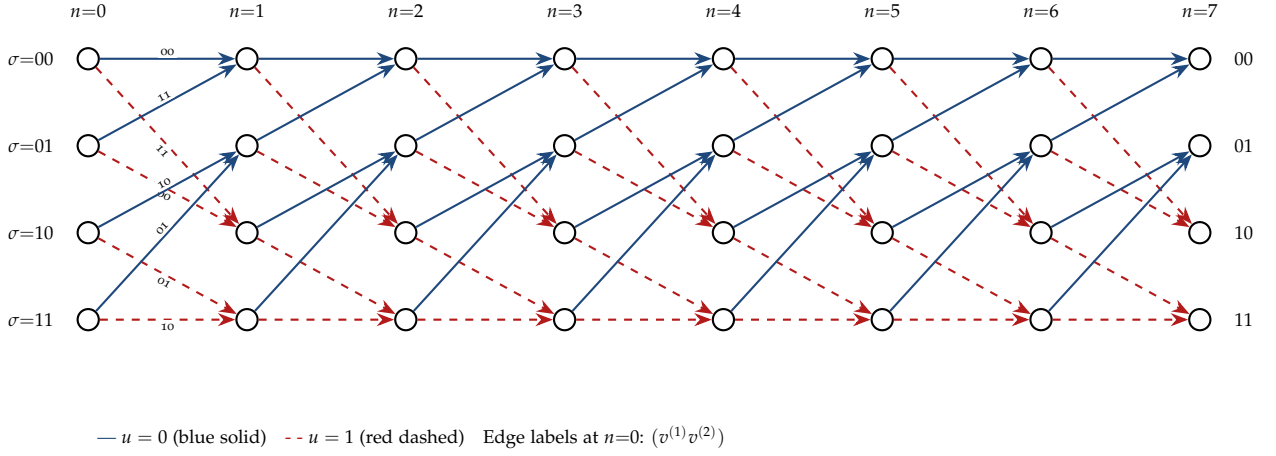


Figure 2: Rate- $\frac{1}{2}$ trellis, 4 lowest states over $n = 0, \dots, 7$. Blue solid: $u = 0$; red dashed: $u = 1$. Edge labels $(v^{(1)}v^{(2)})$ are shown for the first transition only; the pattern repeats identically at every subsequent step. The full code has 64 states; here $\sigma \in \{00, 01, 10, 11\}_2$.

Puncturing and Puncture Matrices

Higher code rates are obtained by *puncturing*: periodically deleting output bits before transmission [2, 8, 18]. Cain et al. [2] showed that rate- $(n-1)/n$ codes can be derived this way from a low-rate mother code without re-designing the decoder; Yasuda et al. [18] extended the approach to high rates with soft-decision Viterbi decoding; and Hagenauer [8] unified the family into rate-compatible punctured convolutional (RCPC) codes. The surviving bits are specified by a binary *puncture matrix* \mathbf{P} , whose two rows correspond to the output streams $v^{(1)}$ and $v^{(2)}$, and whose columns span one period. A 1 means “transmit”; a 0 means “delete”. The serialised puncture mask \mathbf{p} is read column-by-column from \mathbf{P} .

Rate $\frac{1}{2}$ — unpunctured

Both outputs are kept at every step. The period is $L = 2$:

$$\mathbf{P}_{1/2} = \begin{pmatrix} 1 \\ 1 \end{pmatrix}, \quad \mathbf{p} = (1, 1).$$

Rate $\frac{2}{3}$

For every two input bits the encoder produces 4 output bits; 3 are transmitted ($v_1^{(2)}$ is deleted):

$$\mathbf{P}_{2/3} = \begin{pmatrix} 1 & 1 \\ 1 & 0 \end{pmatrix}, \quad \mathbf{p} = (1, 1, 1, 0), \quad L = 4.$$

Code rate = $2/3$ because 2 info bits yield 3 transmitted bits.

Rate 3/4

Three input bits produce 6 outputs; 4 are transmitted:

$$\mathbf{P}_{3/4} = \begin{pmatrix} 1 & 1 & 0 \\ 1 & 0 & 1 \end{pmatrix}, \quad \mathbf{p} = (1, 1, 1, 0, 0, 1), \quad L = 6.$$

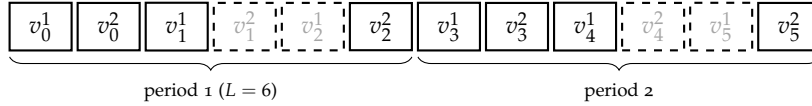
Positions 4 and 5 of the serial stream ($v_2^{(1)}$ and $v_1^{(2)}$) are deleted.

Rate 5/6

Five input bits produce 10 outputs; 6 are transmitted:

$$\mathbf{P}_{5/6} = \begin{pmatrix} 1 & 1 & 0 & 1 & 0 \\ 1 & 0 & 1 & 0 & 1 \end{pmatrix}, \quad \mathbf{p} = (1, 1, 1, 0, 0, 1, 1, 0, 1, 0), \quad L = 10.$$

Figure ?? illustrates the rate-3/4 mask over two full periods. Solid-bordered cells are transmitted; dashed cells are deleted before the channel.



Distance Spectrum: Definitions

Definition 1 (Distance spectrum [12, 15, 17]). *The distance spectrum of a convolutional code is the pair of integer sequences $\{(\alpha_d, \beta_d)\}_{d \geq d_{\text{free}}}$ where α_d counts error events at Hamming distance d from the all-zero codeword, and β_d is the total input Hamming weight of those paths. The smallest d for which $\alpha_d > 0$ is the free distance d_{free} [5, 16], the primary figure of merit for a convolutional code's error-correcting capability.*

BER Bounds from the Distance Spectrum

Union bound on bit-error probability

For the Viterbi decoder [6, 16] over an AWGN channel with BPSK modulation, the pairwise error probability between two codewords at Hamming distance d is [14, 15]

$$P_2(d) = Q\left(\sqrt{2d R_c \frac{E_b}{N_0}}\right),$$

where R_c is the code rate, E_b/N_0 is the information-bit SNR, and $Q(x) = \frac{1}{\sqrt{2\pi}} \int_x^\infty e^{-t^2/2} dt$. Applying the union bound over all error events [12, 16] gives the *union-bound bit-error probability*

$$P_b \lesssim \sum_{d=d_{\text{free}}}^{D_{\text{max}}} \beta_d Q\left(\sqrt{2d R_c \frac{E_b}{N_0}}\right), \quad (3)$$

where $k = 1$ information bit per step is used (absorbed into β_d).

Rate	Mask \mathbf{p}	L	d_{free}
1/4	11	2	10
	1110	4	6
	111001	6	5
	1110011010	10	4

Table 1: 802.11 puncture masks and free distances.

Figure 3: Rate-3/4 mask 111001 over two periods. Solid border: transmitted. Dashed border: deleted before transmission. Superscript indexes the generator (1 or 2); subscript indexes the input-bit time step. 4 of every 6 serial output bits are transmitted, giving rate $\frac{4/2}{6/2} = \frac{2}{3} \cdot \frac{3}{2} = \frac{3}{4}$.

Frame error rate

The frame/event error rate uses the multiplicity directly:

$$P_f \lesssim \sum_{d=d_{\text{free}}}^{D_{\text{max}}} \alpha_d Q\left(\sqrt{2d R_c \frac{E_b}{N_0}}\right). \quad (4)$$

Single-term approximation

Near the waterfall region the leading term dominates:

$$P_b \approx \beta_{d_{\text{free}}} Q\left(\sqrt{2d_{\text{free}} R_c \frac{E_b}{N_0}}\right). \quad (5)$$

Table ?? evaluates the full bound (3) using 10 spectrum terms at several SNR points.

E_b/N_0 (dB)	Rate $\frac{1}{2}$		Rate $\frac{2}{3}$		Rate $\frac{3}{4}$		Rate $\frac{5}{6}$	
	P_b^{UB}	P_f^{UB}	P_b^{UB}	P_f^{UB}	P_b^{UB}	P_f^{UB}	P_b^{UB}	P_f^{UB}
3	1.6×10^{-1}	1.8×10^{-1}	1.4×10^{-1}	1.4×10^{-1}	1.3×10^{-1}	1.1×10^{-1}	1.2×10^{-1}	1.7×10^{-1}
4	4.2×10^{-2}	5.3×10^{-2}	5.1×10^{-2}	5.3×10^{-2}	6.3×10^{-2}	5.5×10^{-2}	8.1×10^{-2}	1.1×10^{-1}
5	4.2×10^{-4}	5.3×10^{-4}	8.7×10^{-3}	9.0×10^{-3}	1.7×10^{-2}	1.5×10^{-2}	4.4×10^{-2}	6.2×10^{-2}
6	5.8×10^{-8}	7.2×10^{-8}	4.4×10^{-4}	4.5×10^{-4}	2.0×10^{-3}	1.7×10^{-3}	1.3×10^{-2}	1.8×10^{-2}
7	$< 10^{-14}$	$< 10^{-14}$	3.6×10^{-6}	3.7×10^{-6}	5.4×10^{-5}	4.7×10^{-5}	1.9×10^{-3}	2.6×10^{-3}
8	$\ll 10^{-20}$	$\ll 10^{-20}$	3.5×10^{-9}	3.6×10^{-9}	2.7×10^{-7}	2.4×10^{-7}	1.4×10^{-4}	2.0×10^{-4}

Table 2: Union-bound BEP (3) and FER (4) using 10 spectrum terms, BPSK over AWGN [14, 16]. The rate- $\frac{1}{2}$ bound collapses rapidly above 5 dB; higher-rate codes require higher SNR for the same error floor because their spectra are denser and d_{free} is smaller.

Notes on bound tightness

The union bound (3) is loose at low SNR (overlapping pairwise events) but tightens rapidly in the waterfall region because $Q(\sqrt{2d_{\text{free}} R_c E_b/N_0})$ decays faster than any polynomial [6]. For the rate- $\frac{1}{2}$ code the single $d = 10$ term (5) is already tight above 5 dB. Higher-rate codes require several more terms because their spectra grow more quickly with d .

Uncoded BPSK has $P_b = Q(\sqrt{2E_b/N_0})$ [14]. The rate- $\frac{1}{2}$ code provides roughly 4–5 dB coding gain at $P_b = 10^{-5}$ [9, 14]; the rate- $\frac{3}{4}$ code provides approximately 2–3 dB, trading protection for bandwidth efficiency. Figure ?? plots both bounds across the full waterfall region.

Bounds for Gray-Coded M-QAM

Channel model

In IEEE 802.11 the BCC-encoded bit stream is interleaved and mapped to M -QAM symbols. Under the standard AWGN channel model, the received complex sample for symbol index k is

$$y_k = \sqrt{E_s} s_k + n_k, \quad n_k \sim \mathcal{CN}(0, N_0), \quad (6)$$

where $s_k \in \mathcal{S}$ is the transmitted symbol from the normalised Gray-coded square M -QAM alphabet [14, 15], and $E_s = m R_c E_b$ with $m = \log_2 M$ bits per symbol.

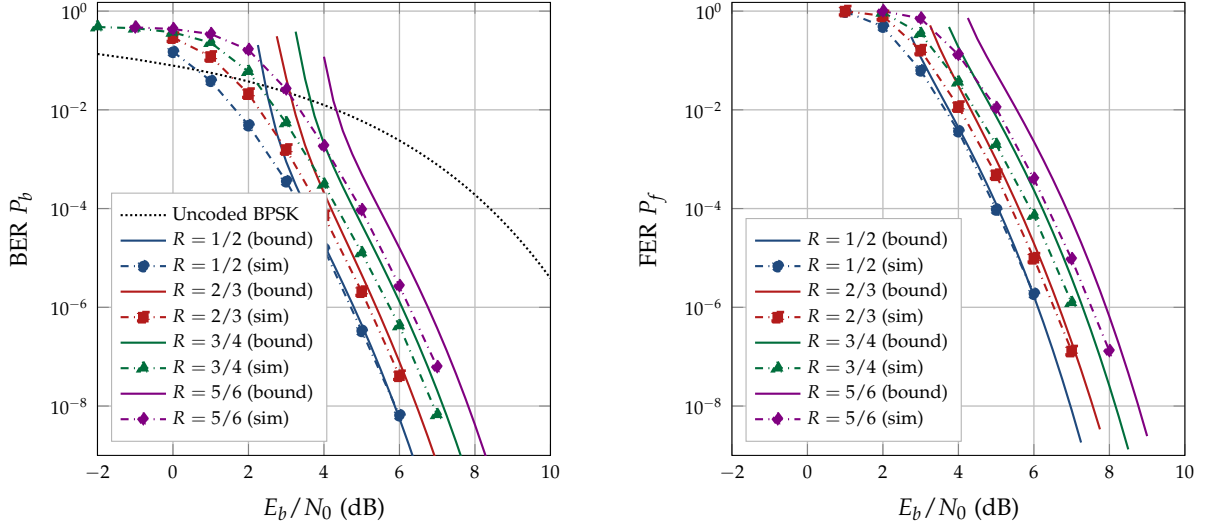


Figure 4: BEP union bound (3) (left) and FER union bound (4) (right, $K = 1024$ information bits) for all four IEEE 802.11 BCC rates over AWGN with QPSK modulation [14, 16]. Lines: union bounds using 30 spectrum terms ($d_{\max} = 130$), solid for both BEP and FER. Markers: Monte Carlo simulation, dot-dashed lines; \bullet $R = \frac{1}{2}$, \blacksquare $R = \frac{2}{3}$, \blacktriangle $R = \frac{3}{4}$, \blacklozenge $R = \frac{5}{6}$. Dotted black: uncoded BPSK $Q\left(\sqrt{2E_b/N_0}\right)$ (BEP panel only). The FER bound lies roughly K/\bar{w} times above the BEP bound ($\bar{w} \approx 3\text{--}7$ per rate); both bounds track the simulation closely in the waterfall region.

Effective SNR factor Δ_M

A Gray-coded soft demapper computes one LLR per coded bit. Under the BICM model [3], the dominant contribution to the pairwise error probability between paths at Hamming distance d uses the minimum intra-constellation bit distance, giving the upper bound [12, 14]

$$P_2(d) \leq Q\left(\sqrt{2R_c d \Delta_M \frac{E_b}{N_0}}\right), \quad (7)$$

where the *modulation penalty factor*

$$\Delta_M = \frac{3m}{2(M-1)}, \quad m = \log_2 M, \quad M \geq 4, \quad (8)$$

captures the reduced per-bit minimum Euclidean distance as the constellation grows. For QPSK ($M = 4$) the formula yields $\Delta_M = 1$, recovering the standard BPSK result; BPSK ($M = 2$) is the underlying binary channel to which (8) does not apply. Table ?? lists the values for the four constellations used in IEEE 802.11 [10].

M	m	Δ_M	Penalty (dB)
4	2	1	0.0
16	4	$2/5 = 0.4$	-4.0
64	6	$2/14 \approx 0.143$	-8.5
256	8	$8/170 \approx 0.047$	-13.3

Union bounds

Substituting (7) into the BPSK bounds replaces E_b/N_0 by $\Delta_M E_b/N_0$, giving the M -QAM BEP and FER union bounds [12, 14]:

$$P_b \leq \sum_{d=d_{\text{free}}}^{\infty} \beta_d Q\left(\sqrt{2R_c d \Delta_M \frac{E_b}{N_0}}\right), \quad (9)$$

$$P_f(K) \leq K \sum_{d=d_{\text{free}}}^{\infty} \alpha_d Q\left(\sqrt{2R_c d \Delta_M \frac{E_b}{N_0}}\right). \quad (10)$$

Table 3: Modulation penalty factor Δ_M (8) and equivalent E_b/N_0 penalty relative to BPSK at the same coded-bit reliability. Each step from QPSK to the next order costs roughly 4–5 dB.

The factor K is the frame length in information bits; it enters because any of the K trellis steps can initiate an error event. Setting $\Delta_M = 1$ (QPSK) recovers the BPSK bounds (3) and (4) exactly. Higher-order QAM shifts the entire waterfall to the right by $10 \log_{10}(1/\Delta_M)$ dB with no change in slope.

The uncoded reference BEP for Gray-coded M -QAM is

$$P_b^{\text{unc}}(M) = \frac{4}{m} \left(1 - \frac{1}{\sqrt{M}}\right) Q\left(\sqrt{\frac{3m}{M-1} \frac{E_b}{N_0}}\right), \quad (11)$$

a tight approximation for $E_b/N_0 \gtrsim 5$ dB [14].

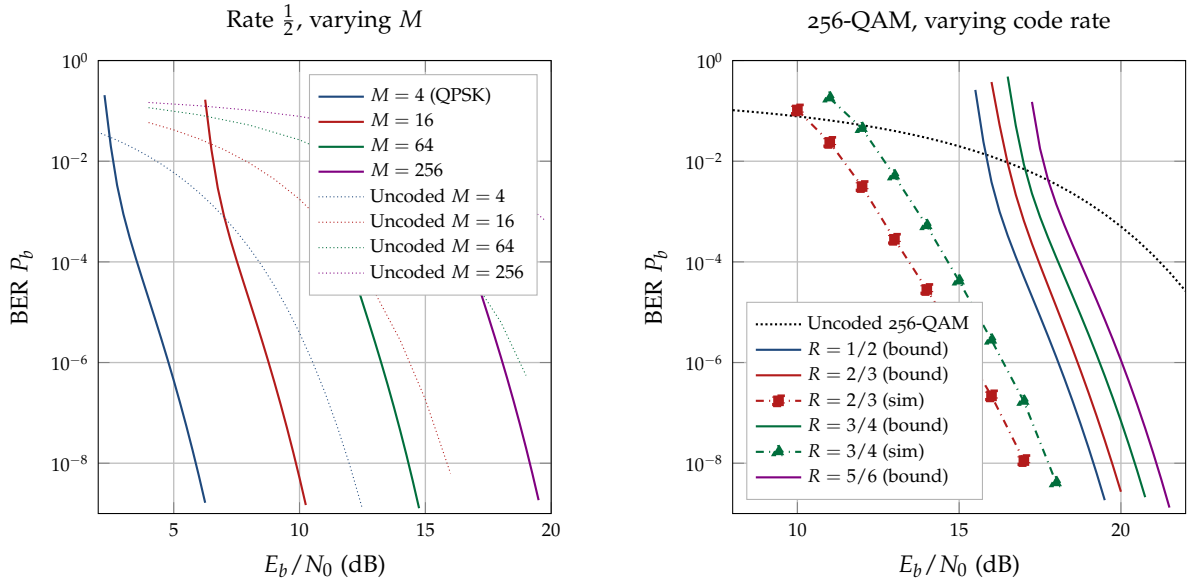


Figure 5: BEP union bounds (9) for Gray-coded M -QAM over AWGN with 30 spectrum terms ($d_{\max} = 130$) [3, 12, 14]. *Left:* code rate $\frac{1}{2}$ fixed; solid lines are coded bounds, dotted lines are uncoded M -QAM references. Each factor-of-4 increase in M shifts the waterfall ≈ 4 –5 dB to the right (see Δ_M , Table ??). *Right:* 256-QAM fixed; all four code rate bounds are shown (solid), with Monte Carlo simulation markers (\bullet , dot-dashed) for $R = 2/3$ and $R = 3/4$. The uncoded 256-QAM reference is shown dotted.

Augmented Trellis and Transfer Function

Why augment the state

For the unpunctured code the transfer function method [12, 17] uses a single 64×64 state space. Puncturing makes the branch weight *phase-dependent*: consecutive encoder steps may contribute differently depending on which bits survive the mask. Augmenting the state with the puncture phase converts this into a time-invariant problem [8]:

Definition 2 (Augmented state). (σ, ϕ) where $\sigma \in \{0, \dots, 63\}$ is the encoder state and $\phi \in \{0, \dots, L-1\}$ is the position in the puncture mask.

For rate- $\frac{3}{4}$ ($L = 6$) the augmented space has $64 \times 6 = 384$ states.

Branch weights

Each branch carries weight $D^d N^u$ where $d = p_\phi v^{(1)} + p_{(\phi+1) \bmod L} v^{(2)}$ counts transmitted 1-bits, and the phase advances by 2 per step.

State partitioning

Let $\mathcal{S} = \{(\sigma, \phi) \neq (0, 0)\}$. Branches split into: **E**: START \rightarrow \mathcal{S} ; **Q**: $\mathcal{S} \rightarrow \mathcal{S}$; **R**: $\mathcal{S} \rightarrow$ START.

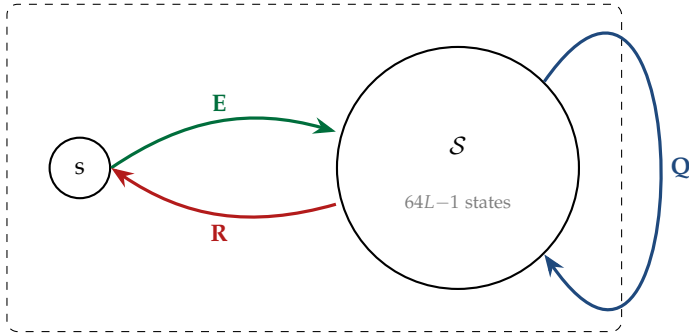


Figure 6: E/Q/R partition of the augmented trellis. The transfer function sums over all first-return paths from START to START.

Computing the Transfer Function

First-return generating function

The first-return transfer polynomial [1, 12, 17] is

$$T(D, N) = \mathbf{E}^\top (\mathbf{I} - \mathbf{Q})^{-1} \mathbf{R}, \quad \alpha_d = [D^d] T(D, 1), \quad \beta_d = [D^d] \frac{\partial T}{\partial N} \Big|_{N=1}.$$

Neumann series (truncated)

The Neumann (geometric) series identity [12, 15]

$$\mathbf{x} = (\mathbf{I} - \mathbf{Q})^{-1} \mathbf{R} = \sum_{k \geq 0} \mathbf{Q}^k \mathbf{R}$$

avoids explicit matrix inversion. Each \mathbf{Q} -multiplication raises the minimum degree by at least 1, so the sum terminates within d_{\max} steps.

Implementation notes

Sparse polynomials. Dict[int \rightarrow (count, weight)]: only non-zero distances stored.

Combined multiply. $(c_1, w_1) \cdot (c_2, w_2) = (c_1 c_2, w_1 c_2 + w_2 c_1)$ tracks both α and β in one pass.

Early termination. Iteration halts when all polynomial terms exceed d_{\max} .

Pseudocode

Require: Puncture mask $\mathbf{p} \in \{0, 1\}^L$, max distance d_{\max}

Ensure: $d_{\text{free}}, \{\alpha_d\}, \{\beta_d\}$ for $d \leq d_{\max}$

- 1: **for** each augmented state (σ, ϕ) and $u \in \{0, 1\}$ **do**
- 2: Compute (σ', ϕ') , outputs $(v^{(1)}, v^{(2)})$ via (1)–(2)
- 3: $d \leftarrow p_\phi v^{(1)} + p_{(\phi+1) \bmod L} v^{(2)}$; $\text{pol} \leftarrow \{d \mapsto (1, u)\}$
- 4: Route pol to **E**, **Q**, or **R** according to src/dst vs. **START**
- 5: **end for**
- 6: $\mathbf{x} \leftarrow \mathbf{0}$; $\text{term} \leftarrow \mathbf{R}$
- 7: **repeat**
- 8: $\mathbf{x} += \text{term}$; $\text{term} \leftarrow \mathbf{Q} \cdot \text{term}$ (sparse, truncate at d_{\max})
- 9: **until** $\text{term} = \mathbf{0}$
- 10: $T \leftarrow \mathbf{E}^\top \mathbf{x}$; remove $T[0]$
- 11: $d_{\text{free}} \leftarrow \min(\text{keys}(T))$; $\alpha_d \leftarrow T[d].\text{count}$; $\beta_d \leftarrow T[d].\text{weight}$

Figure 7: All-zero self-loop ($\text{START} \rightarrow \text{START}, u = 0$) is excluded so only non-trivial error events are counted.

Full Distance Spectrum Tables

Tables ??–?? list the distance spectrum for each of the four IEEE 802.11 BCC rates, computed at $d_{\max} = 200$ by all three provided implementations. The leading entries near d_{free} dominate the union bound (3) at practical SNRs [12, 14]; the rapidly growing tail is tabulated for completeness.

Complexity and Correctness

State space. $64L$ augmented states [8]; for $L \leq 10$ the matrix is at most 639×639 . The Neumann iteration converges in milliseconds on any modern workstation.

Convergence. $\mathbf{Q}^k \mathbf{R}$ has minimum polynomial degree $\geq k$ (the all-zero path is excluded by dropping the **START** self-loop [12, 17]), guaranteeing termination within d_{\max} steps.

Validation. Published reference values [10, 14] ($d_{\text{free}} = 10, \alpha_{10} = 11, \beta_{10} = 36$ for rate- $\frac{1}{2}$) are reproduced exactly by all three implementations.

Method: Augmented-Trellis First-Return Series

The full descriptive title of the technique used throughout this report is the **augmented-trellis first-return series expansion**. “Augmented trellis”: the encoder state is extended by a puncture-phase coordinate [8, 18], converting a phase-dependent problem into a time-invariant graph. “First-return”: only paths from **START** back

Rate $\frac{1}{2}$, $d_{\text{free}} = 10$		
d	α_d	β_d
10	11	36
12	38	211
14	193	1404
16	1331	11633
18	7275	77433
20	40406	502690
22	234969	3322763
24	1337714	21292910
26	7594819	134365911
28	43375588	843425871
30	247339453	5245283348
32	1409277901	32372937519
34	8034996288	198723833069
36	45808756116	1213657958889
38	261128775464	7378557447583
40	1488634502286	4468630466721
42	8486419243793	269700526164453
44	48378617913225	1622729997782985
46	275793790396626	9736706163099939
48	1572231420375534	58276780724903312
50	8962880896223488	348013358443369656
52	51095054431014717	2073963288833171453
54	291279733217405452	12336364663874535729
56	1660510362328999082	73252242728489893106
58	9466139591359800558	434271414857187001700
60	53964013243208867416	2570753624392467445784
62	307634876470723955762	15197254111652957956012
64	1753746820351580399624	89725716153372815432783
66	9997656840401781321694	529118969577464553987962
68	56994054713893565476484	3116793898985013529095287
70	324908358143739422211879	18340524278975143091254596
72	1852218477505497507791900	107818193462006470300574577
74	10559018266445912586742730	633248620007255756144580769
76	6019423091245913771773409	3716048802987112205321093900
78	343151734741456193472066807	21788866274369339795691938329
80	1956219246813370209261798213	127659548322985097263197345800
82	11151899740282547158768192994	747403707510664069605252957557
84	63574094785214431866818170525	4372772741086158690229034611083
86	362419464118062623197028805210	25566629266561432354938081678201
88	2066059586301199607386445446232	149389136373987711925267978784505

to START (without revisiting it) are enumerated—exactly the set of error events entering the union bound of Viterbi [16]. “Series expansion”: the Neumann series $(I - Q)^{-1} = \sum_k Q^k$ avoids explicit matrix inversion [1, 12].

This is closely related to the *transfer function* or *state diagram* method described in Lin & Costello [12], Viterbi & Omura [17], and Blahut [1]; and to the *generating function* approach in Ryan & Lin [15]. The phase augmentation for punctured codes is due to Hagenauer [8] and Yasuda et al. [18]; the free-distance optimality of the 133₈/171₈ generators was established by Odenwalder [13] and documented for Viterbi-decoded satellite systems by Heller & Jacobs [9].

Spectrum Toolkit

Three independent implementations are provided, all producing bit-identical results. Source code and build instructions are available at https://github.com/geekymode/bcc_spectrum [7].

python/bcc_spectrum.py Pure Python 3, standard library only. No external dependencies.

julia/bcc_spectrum.jl Julia with typed dictionaries and in-place

Table 4: Distance spectrum for rate $\frac{1}{2}$, first 40 non-zero terms. Only even- d terms appear owing to the odd-even distance structure of the unpunctured code [12, 17]. Both α_d (event multiplicity) and β_d (total input-bit weight) grow exponentially with d . The first few rows near d_{free} dominate the union-bound BEP (3).

Rate $\frac{2}{3}$, $d_{\text{free}} = 6$		
d	α_d	β_d
6	1	3
7	16	70
8	48	285
9	158	1276
10	642	6160
11	2435	27128
12	9174	117019
13	34705	498860
14	131585	2103891
15	499608	8784123
16	1893179	36328084
17	7172729	149215136
18	27191646	609374214
19	103077011	2475565587
20	390696502	10011487814
21	1480891596	40328889729
22	5613272624	161890464724
23	21276960168	647849333879
24	80649275876	2585310552363
25	305696805990	10290999621644
26	1158729619748	40870598781266
27	4392111993691	161979866397621
28	16648093424227	640744298836396
29	63103811287025	2530171149917233
30	239192038606689	9975074654637651
31	906646220176741	39267783332904885
32	3436599953926219	154368148990251773
33	13026270800979961	606069217780505410
34	49375468291633374	2376664159970176069
35	187155396191213743	9309547543710430089
36	709403747993606556	36428001853950581850
37	2688961620804198202	142402017658290454051
38	10192382858882494599	556155757695350210952
39	38633749008587856293	2170198700519724466025
40	146439412940381687661	8461485632028557640931
41	555071723869022381011	32965323736976789411788
42	2103973325619741975380	128336338609792333679995
43	7975012173381708369090	499275312124292023982821
44	30228909459430820775734	1941082510012205927466204
45	114581262979693073017508	7541809059515936836327070

polynomial arithmetic.

`cpp/bcc_spectrum.cpp + bcc_spectrum.h` C++17 reusable library with a command-line driver in `main.cpp`.

Python

Python — command line & library usage

```
# Run from terminal: d_max=30, show 5 terms per rate
python3 python/bcc_spectrum.py 30 5

# Library API
from python.bcc_spectrum import compute_spectrum, PUNCTURE_MASKS
dfree, alpha, beta = compute_spectrum(PUNCTURE_MASKS["1/2"], d_max=60)
print(dfree, alpha[10], beta[10]) # 10 11 36

# Custom puncture mask
my_mask = [1, 1, 0, 1, 1, 0]
dfree, alpha, beta = compute_spectrum(my_mask, d_max=80)
```

Table 5: Distance spectrum for rate $\frac{2}{3}$, first 40 non-zero terms. Puncturing one bit per period reduces d_{free} from 10 to 6 and introduces odd- d terms [2, 18]. Both α_d (event multiplicity) and β_d (total input-bit weight) grow exponentially with d . The first few rows near d_{free} dominate the union-bound BEP (3).

Rate $\frac{3}{4}$, $d_{\text{free}} = 5$		
d	α_d	β_d
5	8	42
6	31	201
7	160	1 492
8	892	10 469
9	4 512	62 935
10	23 307	379 644
11	121 077	2 253 373
12	625 059	13 073 811
13	3 234 886	75 152 755
14	16 753 077	428 005 675
15	86 686 071	2 415 121 123
16	448 565 858	13 534 984 705
17	2 321 546 552	75 422 690 722
18	12 014 661 684	418 134 779 192
19	62 177 678 298	2 307 775 877 171
20	321 782 203 428	12 687 767 739 589
21	1 665 294 549 473	69 515 274 896 547
22	8 618 250 200 425	379 697 527 047 278
23	44 601 241 330 678	2 068 214 528 915 872
24	230 820 838 592 718	11 237 531 722 373 744
25	1 194 546 586 395 172	60 920 601 474 530 625
26	6 182 030 185 381 023	329 581 239 552 578 272
27	31 993 308 832 099 435	1 779 680 104 530 834 762
28	165 572 117 751 393 610	9 593 328 859 682 938 761
29	856 870 607 034 189 819	51 630 169 441 762 663 061
30	4 434 485 984 875 218 930	277 457 746 783 477 047 589
31	22 949 399 628 811 599 853	1 489 003 802 780 537 995 255
32	118 767 980 116 369 449 256	7 980 719 884 803 595 786 399
33	614 649 329 566 088 851 154	42 724 114 238 398 358 327 533
34	3 180 939 829 090 587 663 771	228 466 515 787 057 620 239 973
35	16 462 034 057 400 611 109 436	1 220 453 061 059 539 812 179 628
36	85 194 495 923 024 617 552 504	6 513 229 164 273 472 492 588 230
37	440 899 472 705 962 824 580 787	34 727 509 242 517 223 649 661 501
38	2 281 747 698 919 298 191 628 292	185 001 803 203 789 088 989 606 300
39	11 808 525 262 158 996 793 797 400	984 746 488 048 876 648 491 885 530
40	61 111 607 095 328 770 658 831 016	5 237 673 761 317 170 635 847 174 896
41	316 265 447 112 328 542 272 132 605	27 837 856 663 491 539 147 883 618 742
42	1 636 740 347 560 052 011 522 600 685	147 853 948 302 437 837 631 540 003 889
43	8 470 476 271 723 617 072 730 452 262	784 774 762 490 643 725 716 187 973 867
44	43 836 500 014 672 964 072 435 134 751	4 162 805 915 963 836 391 011 696 811 539

Julia

Julia — command line & interactive usage

```
# Run from terminal: d_max=30, show 5 terms per rate
julia julia/bcc_spectrum.jl 30 5

# REPL / script
include("julia/bcc_spectrum.jl")
dfree, alpha, beta = compute_spectrum(PUNCTURE_MASKS["3/4"], 60)
println(dfree, " ", alpha[5], " ", beta[5]) # 5 8 42
```

Table 6: Distance spectrum for rate $\frac{3}{4}$, first 40 non-zero terms. Two output bits per period are deleted; d_{free} falls to 5 [18]. Both α_d (event multiplicity) and β_d (total input-bit weight) grow exponentially with d . The first few rows near d_{free} dominate the union-bound BEP (3).

Rate $\frac{5}{6}$, $d_{\text{free}} = 4$		
d	α_d	β_d
4	14	92
5	69	528
6	654	8694
7	4996	79453
8	39699	792114
9	315371	7375573
10	2507890	67884974
11	19921920	610875423
12	158275483	5427275376
13	1257455600	47664215639
14	9990453938	414847451604
15	79372452075	3583040670062
16	630602872400	30748409619146
17	5010053531956	262418568123539
18	39804179617382	2228895012849046
19	316238637713112	18852439937923866
20	2512471862922901	158870376816716859
21	19961238706464034	1334424696449318311
22	158589257850835062	11175609534518649264
23	1259969536714370401	93347351761800157709
24	10010282258845090282	777849869010260843014
25	79530296563407917449	6467657099669465163457
26	631857115254729072678	53670754342729722819253
27	5020016664677983514074	444569568207478822347564
28	39883332331658123789262	3676345005910658028271387

Table 7: Distance spectrum for rate $\frac{5}{6}$, first 25 non-zero terms. Four output bits per period are deleted; $d_{\text{free}} = 4$ is the lowest of the four standard rates [8, 10]. Both α_d (event multiplicity) and β_d (total input-bit weight) grow exponentially with d . The first few rows near d_{free} dominate the union-bound BEP (3).

C++

C++17 — build, run & library usage

```
# Build
g++ -std=c++17 -O2 -o bcc_spectrum cpp/bcc_spectrum.cpp cpp/main.cpp
# or: make

# Run from terminal: d_max=30, show 5 terms per rate
./bcc_spectrum 30 5

// Library API in your own code
#include "bcc_spectrum.h"
auto [dfree, alpha, beta] = bcc::compute_spectrum(bcc::mask_half(),
        60);
// dfree=10 alpha[10]=11 beta[10]=36

auto [df23, a23, b23] = bcc::compute_spectrum(bcc::mask_two3(), 60);
```

Sample output ($d_{\max}=30$, 5 terms per rate)

```

Terminal output — identical across all three implementations

IEEE 802.11 BCC Distance Spectrum
K=7, generators 133_8 / 171_8
d_max=30, showing first 5 non-zero terms
=====

Rate 1/2 (puncture period = 2)
d_free = 10
  d             alpha_d             beta_d
  ---          -
  10            11                    36
  12            38                    211
  14            193                   1,404
  16            1,331                 11,633
  18            7,275                 77,433

Rate 2/3 (puncture period = 4)
d_free = 6
  d             alpha_d             beta_d
  ---          -
  6             1                    3
  7             16                   70
  8             48                   285
  9             158                  1,276
  10            642                  6,160

Rate 3/4 (puncture period = 6)
d_free = 5
  d             alpha_d             beta_d
  ---          -
  5             8                    42
  6             31                   201
  7             160                  1,492
  8             892                  10,469
  9             4,512                 62,935

Rate 5/6 (puncture period = 10)
d_free = 4
  d             alpha_d             beta_d
  ---          -
  4             14                    92
  5             69                   528
  6             654                   8,694
  7             4,996                 79,453
  8             39,699                792,114

```

References

- [1] R. E. Blahut. *Theory and Practice of Error Control Codes*. Addison-Wesley, Reading, MA, USA, 1983.
- [2] J. B. Cain, G. C. Clark Jr., and J. M. Geist. Punctured convolutional codes of rate $(n-1)/n$ and simplified maximum likelihood decoding. *IEEE Transactions on Information Theory*, 25(1):97–100, Jan. 1979.
- [3] G. Caire, G. Taricco, and E. Biglieri. Bit-interleaved coded modulation. *IEEE Transactions on Information Theory*, 44(3):927–946, 1998. doi: 10.1109/18.669123.
- [4] Consultative Committee for Space Data Systems. Telemetry channel

- coding. Technical Report CCSDS 131.0-B-3, CCSDS, Washington, DC, USA, 2013. Blue Book.
- [5] G. D. Forney Jr. Convolutional codes I: Algebraic structure. *IEEE Transactions on Information Theory*, 16(6):720–738, Nov. 1970.
- [6] G. D. Forney Jr. The Viterbi algorithm. *Proceedings of the IEEE*, 61(3):268–278, Mar. 1973.
- [7] geekymode. bcc_spectrum: Distance spectrum and performance bounds for IEEE 802.11 BCC. GitHub repository, 2024. URL https://github.com/geekymode/bcc_spectrum. https://github.com/geekymode/bcc_spectrum. Python, Julia, and C++17 implementations.
- [8] J. Hagenauer. Rate-compatible punctured convolutional codes (RCPC codes) and their applications. *IEEE Transactions on Communications*, 36(4):389–400, Apr. 1988.
- [9] J. A. Heller and I. M. Jacobs. Viterbi decoding for satellite and space communication. *IEEE Transactions on Communication Technology*, 19:835–848, 1971.
- [10] IEEE 802.11-2020. IEEE std 802.11-2020: IEEE standard for information technology — wireless LAN medium access control (MAC) and physical layer (PHY) specifications. IEEE, New York, NY, USA, 2021. Revision of IEEE Std 802.11-2016.
- [11] IEEE 802.11 Working Group. IEEE 802.11bn (ultra high reliability). IEEE Standards Association, ongoing task group, 2024. Wi-Fi 8; see <https://www.ieee802.org/11/>.
- [12] S. Lin and D. J. Costello Jr. *Error Control Coding*. Pearson Prentice Hall, Upper Saddle River, NJ, USA, 2nd edition, 2004.
- [13] J. P. Odenwalder. *Optimal Decoding of Convolutional Codes*. PhD thesis, University of California, Los Angeles, 1970.
- [14] J. G. Proakis. *Digital Communications*. McGraw-Hill, New York, NY, USA, 4th edition, 2001.
- [15] W. E. Ryan and S. Lin. *Channel Codes: Classical and Modern*. Cambridge University Press, Cambridge, UK, 2009.
- [16] A. J. Viterbi. Error bounds for convolutional codes and an asymptotically optimum decoding algorithm. *IEEE Transactions on Information Theory*, 13(2):260–269, Apr. 1967.
- [17] A. J. Viterbi and J. K. Omura. *Principles of Digital Communication and Coding*. McGraw-Hill, New York, NY, USA, 1979.
- [18] Y. Yasuda, K. Kashiki, and Y. Hirata. High-rate punctured convolutional codes for soft decision Viterbi decoding. *IEEE Transactions on Communications*, 32(3):315–319, Mar. 1984.